Talanta 137 (2015) 43–54

Contents lists available at ScienceDirect

Talanta

journal homepage: www.elsevier.com/locate/talanta

Review

Recent applications of hyperspectral imaging in microbiology

Aoife A. Gowen [a,*], Yaoze Feng [d], Edurne Gaston [b], Vasilis Valdramidis [c]

[a] UCD School of Biosystems Engineering, College of Engineering and Architechture, University College Dublin, Dublin 4, Ireland
[b] IRIS-Innovació iRecerca Industrial iSostenible, Avda. Carl Friedrich Gauss nº 11, 08860 Castelldefels, Barcelona, Spain
[c] Department of Food Studies and Environmental Health, Faculty of Health Sciences, University of Malta, Msida MSD 2080, Malta
[d] College of Engineering, Huazhong Agricultural University, Wuhan, Hubei, China

ARTICLE INFO

Article history:
Received 27 August 2014
Received in revised form
5 January 2015
Accepted 9 January 2015
Available online 16 January 2015

Keywords:
Hyperspectral chemical imaging
Imaging spectroscopy
Spectral imaging
Microbiology
Raman
NIR
FTIR

ABSTRACT

Hyperspectral chemical imaging (HSI) is a broad term encompassing spatially resolved spectral data obtained through a variety of modalities (e.g. Raman scattering, Fourier transform infrared microscopy, fluorescence and near-infrared chemical imaging). It goes beyond the capabilities of conventional imaging and spectroscopy by obtaining spatially resolved spectra from objects at spatial resolutions varying from the level of single cells up to macroscopic objects (e.g. foods). In tandem with recent developments in instrumentation and sampling protocols, applications of HSI in microbiology have increased rapidly. This article gives a brief overview of the fundamentals of HSI and a comprehensive review of applications of HSI in microbiology over the past 10 years. Technical challenges and future perspectives for these techniques are also discussed.

Contents

* Tel.: +353 1 7167675.
E-mail address: aoife.gowen@ucd.ie (A.A. Gowen).

http://dx.doi.org/10.1016/j.talanta.2015.01.012
0039-9140/

1. Introduction

Despite advances in sampling and the development of rapid and automated techniques in microbiology, alternative analytical techniques that can be implemented on-line or can provide results in shorter time frames have been or are currently being investigated, including computer vision, spectroscopic methods, molecular and electronic noses and DNA-based methods. The assurance of microbial safety is of utmost importance for many industries, not least the food industry. This is not only because products of high quality and safety are increasingly expected and demanded by the consumers, but also because food safety legislation is more and more stringent [1]. The need for accurate, fast and objective food inspection methods that ensure safe production throughout the entire production process continues to grow. Microbial safety assurance methods have traditionally involved sampling and classical microbiological analyses, which are laborious and time consuming, and do not offer immediate results.

Hyperspectral chemical imaging (HSI), also known as spectral imaging or imaging spectroscopy, goes beyond conventional imaging and spectroscopy through obtaining spatially resolved spectra from an object. Similar to conventional spectroscopic techniques, HSI can be carried out in reflectance, transmission, scattering, transflectance or fluorescence modes. However, the added spatial dimension enables the mapping of chemical components in a sample, which is useful for non-homogeneous samples. HSI has been applied in many diverse and applied areas of analytical chemistry, such as food, agriculture and pharmaceuticals. More recently, HSI modalities have been applied to microbiology. A wide range of studies have been carried out, from understanding chemical reactions within bacterial cells via Raman HSI through to predicting total viable counts on food surfaces using Near infrared HSI. It is thus timely to review the recent applications of HSI in microbiology. These applications can be grouped into three major categories: (1) fundamental papers where HSI is used to gain information on biochemical processes of relevance to microorganisms; (2) applied papers where HSI is used to detect and identify microorganisms of concern at a microscopic scale, usually grown on "artificial" substrates such as stainless steel, silver or selective agars; (3) applied papers where HSI is used to detect microorganisms of concern at a macroscopic scale, grown on "real" substrates such as food or typical food preparation surface (e.g. formica). Using these broad categories, the remainder of this paper is organized as follows: Section 2 provides an overview of typical instrumentation in HSI is presented, with special consideration of the challenges inherent to the application of HSI to microbial samples; Section 3 is a brief overview of techniques typically used to analyse data arising from HSI experiments; Section 4 provides an overview of the state of the art in the application of HSI to microbiology, including critical reviews of the literature; Section 5 summarises the limitations and future perspectives for HSI from a microbiologists perspective and this is followed by the main conclusions in Section 6.

2. Instrumentation

Hyperspectral chemical imaging techniques are available for most traditionally single point spectroscopic methods (e.g. flourescence, visible (Vis), infrared (IR), Fourier-transform IR (FTIR), near infrared (NIR), Raman spectroscopy), although the instrumentation required for each modality varies significantly. However, the typical core components of any HSI system are: light source, wavelength modulation system and detector.

2.1. Light sources

In Vis–NIR HSI systems, the sample/target is usually diffusely illuminated by a tungsten-halogen (TH) light source. These broadband sources cover a wide wavelength range, from 400 to 2500 nm and are low cost [2]. However, the heat generated by TH bulbs is significant and may alter or even burn the sample. This is an important consideration in imaging live microbial samples or foods. To overcome this issue, fiber optic line lights are often used to provide distance between the TH bulb and sample (an example is the set-up used in [3]). Many other types of light sources are also used such as light emitting diodes (LED) which can cover a wide spectral range, from the visible to the near-infrared region. LED light sources have some advantages with respect to TH bulbs due to their small sizes, long lifespan and prevention of sample heating. However, LEDs covering the NIR range are currently more expensive than TH sources and LEDs only provide narrow wavebands of light, making them more suitable for multi-spectral imaging. Vis–NIR hyperspectral fluorescence imaging, useful for identifying biofilms on foods, is typically carried out using UV-A (365 nm) lamps as light sources [4,5].

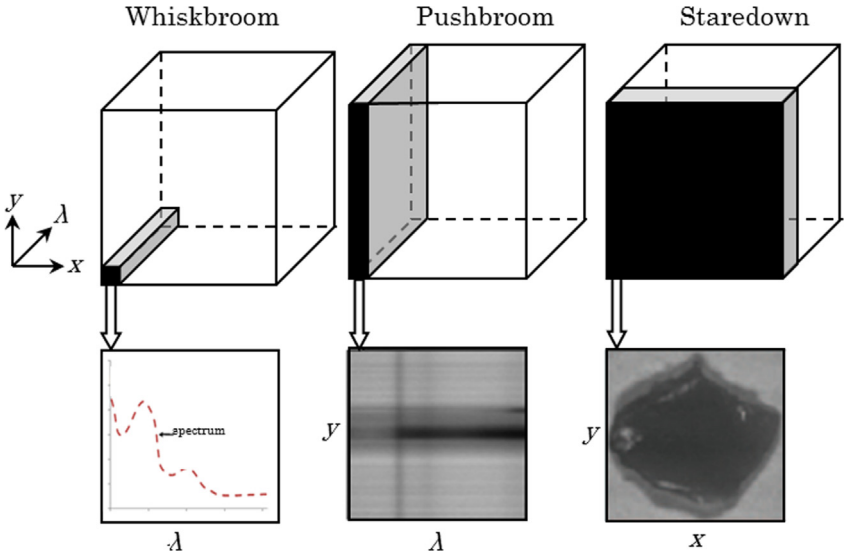

Fig. 1. Schematic showing three working modes of hyperspectral imaging systems taking imaging a chicken breast fillet as an example. Black areas in the upper row denote detected portion of a chicken sample in respective modes and the lower row shows corresponding obtained data during each scan.

Illumination in the MIR is commonly provided by broadband globar (thermal) light sources, such as heated silicon carbide. Aqueous samples such as live microbial cells are highly absorbing in the MIR wavelength range, resulting in a low signal to noise ratio (SNR). Various methods have been proposed to overcome this limitation, such as the use of attenuated total reflection imaging [6] or the use of synchrotron radiation. Synchrotron radiation is up to 1000 times brighter than conventional thermal sources, allowing faster image acquisition with higher SNR [7,8]. However, the low availability and high cost of synchrotrons have limited their use in HSI. In addition, consideration of the influence of the high energy output of synchrotron light sources on sample stability (especially in the case of live microbial samples) is required.

Lasers are commonly used as light sources for Raman scattering measurements. Selection of appropriate excitation wavelength is important, especially for biological samples where auto-fluorescence may completely dominate the signal [9]. Longer excitation wavelengths normally lead to reduced fluorescence but also lower Raman scattering. Most studies reviewed in this paper employed an excitation wavelength of 532 [10–12] or 785 nm [13,14], with the lower wavelength excitation (532 nm) typically requiring a photobleaching step to reduce autofluorescence [15]. Raman HSI often suffers from a low signal to noise ratio, and it is of great importance to develop enhancement techniques to improve signal quality while maintaining fast signal acquisition. Enhancement of the inherently weak Raman signal can be achieved by surface enhancement, i.e. the use of substrates which enhance the Raman signal. Molecular species adsorbed to certain roughened surfaces (e.g. silver or gold) experience signal enhancement up to the order 10^{10}.

2.2. Wavelength modulation

The core component of a HSI system is the light dispersion set-up. Devices available for wavelength dispersion include imaging spectrographs, bandpass filter wheels and tunable filters. These devices can efficiently separate broadband incident lights into different wavelengths so that detectors can record light changes in specific wavelengths with associated spatial information after light-matter interaction. Fourier transform infrared (FTIR) based-HSI systems are commonly used in mid infrared microscopic imaging.

2.3. Detectors

The detector employed is generally optimised for the modality required. For example, HSI systems operating in the visible–very near infrared (Vis–vNIR (400–1000 nm)) range typically utilize cameras with charge coupled device (CCD) or complementary metal oxide semiconductor (CMOS) sensors. Both types of detectors are sensitive in the wavelength range 300–1000 nm, but typically experience a sharp decrease in quantum efficiency below 400 nm and above 900 nm [15]. Electron multiplying CCD (EMCCD) detectors improve the signal to noise ratio and can thus decrease the image acquisition time, which is important for microbiological samples that may be sensitive to heat or photodegradation due to exposure to the light source. Longer wavelength systems (e.g. in the NIR range, 1000–2500 nm) require more expensive detectors, for example Indium Gallium Arsenide (InGaAs) or, mercury cadmium telluride (MCT) detectors. These can be arranged in as a matrix (i.e. focal plane array (FPA)), line or single point, depending on the image acquisition procedure (described in more detail below). Typically, MCT detectors are sensitive in a wider wavelength region than InGaAs (e.g. 900–2500 nm versus 900–1700 nm, respectively [16]), However, longer wavelength InGaAs detectors (up to 2500 nm) are available and cooled MCT detectors are available with sensitivity into the IR (e.g. up to 20 μm [17]). Cooling the detector using liquid nitrogen vastly improves the signal to noise ratio achievable in the MIR.

The three most common ways of obtaining HSI data are described below and further elucidated in Fig. 1:

- **"Whiskbroom" or "point mapping":** a spectrum is acquired at a single spatial location, then the sample is moved underneath the detector using a computer controlled translation stage and the next spectrum is acquired. This procedure is repeated for each spatial position at which spectral data is required. This technique is commonly used for Raman HSI and is typically the most time consuming way to obtain HSI data.
- **"Pushbroom" or "line scanning":** HSI data is obtained from contiguous lines of the sample by relative movement between the sample and detector. This technique is commonly used in Vis-NIR HSI. It is usually x100 times faster than point mapping and is convenient to implement in conveyor belt systems.
- **"Staredown" or "staring face":** HSI data is is obtained by collecting a sequence of images of the sample, one wavelength band at a time. This is the only "true" imaging technique of the three methods shown in Fig. 1.

3. Data analysis

Hyperspectral images are data-rich, typically containing hundreds of thousands of spectra, resulting in megabytes or gigabytes of data. The general aim in data analysis is usually to reduce the dimension of data while retaining sufficient information to classify and or quantify important chemical or physical areas of a scene. HSI datasets are commonly called "hypercubes" (see graphical abstract): three dimensional cubes of data where each slice of the cube represents an image of the sample at a certain waveband. The wealth of spatial and spectral information contained within hypercubes is amenable to data analysis techniques developed by the signal processing, image processing and spectroscopy communities. Although it is outside of the scope of the present paper to describe the details of each technique, here we give a broad overview of methods used and the references contain further detail (e.g. [18–20]).

The main steps involved in hyperspectral image analysis are shown in Fig. 2. Starting with the raw hypercube data, preprocessing is required to remove non-chemical biases and unwanted variation from the spectral and spatial information and to prepare the data for further processing [21]. Detectors used in HSI systems (especially InGaAs detectors commonly used in NIR HSI systems) are prone to dead or non-responsive pixels and spikes due to cosmic radiation. These should be identified and removed prior to further analysis [22]. Noise in the spectra may be decreased by smoothing methods such as median filtering and Savitsky Golay (SG) smoothing, which can also be applied in the spatial domain.

The natural morphology of biological products, such as food or microbial colonies grown on agar, and/or non-uniform lighting are common sources of unwanted spectral variation in hypercubes. Should modifications to the lighting system not be feasible, spectral pre-processing techniques (e.g. standard normal variate (SNV) pre-preprocessing, SG derivatives) may be applied to overcome such effects [23]. However, care must be exercised when applying pretreatments such as multiplicative scatter correction which may produce additional outliers [24]. After dealing with such sources of variation, it may be necessary to remove the image background (i.e. the portion of the image field of view not containing the sample). Thresholding the hypercube (i.e. setting to zero all pixels below or above a certain threshold) at a wavelength that provides high contrast between the sample and background is a simple way to do this.

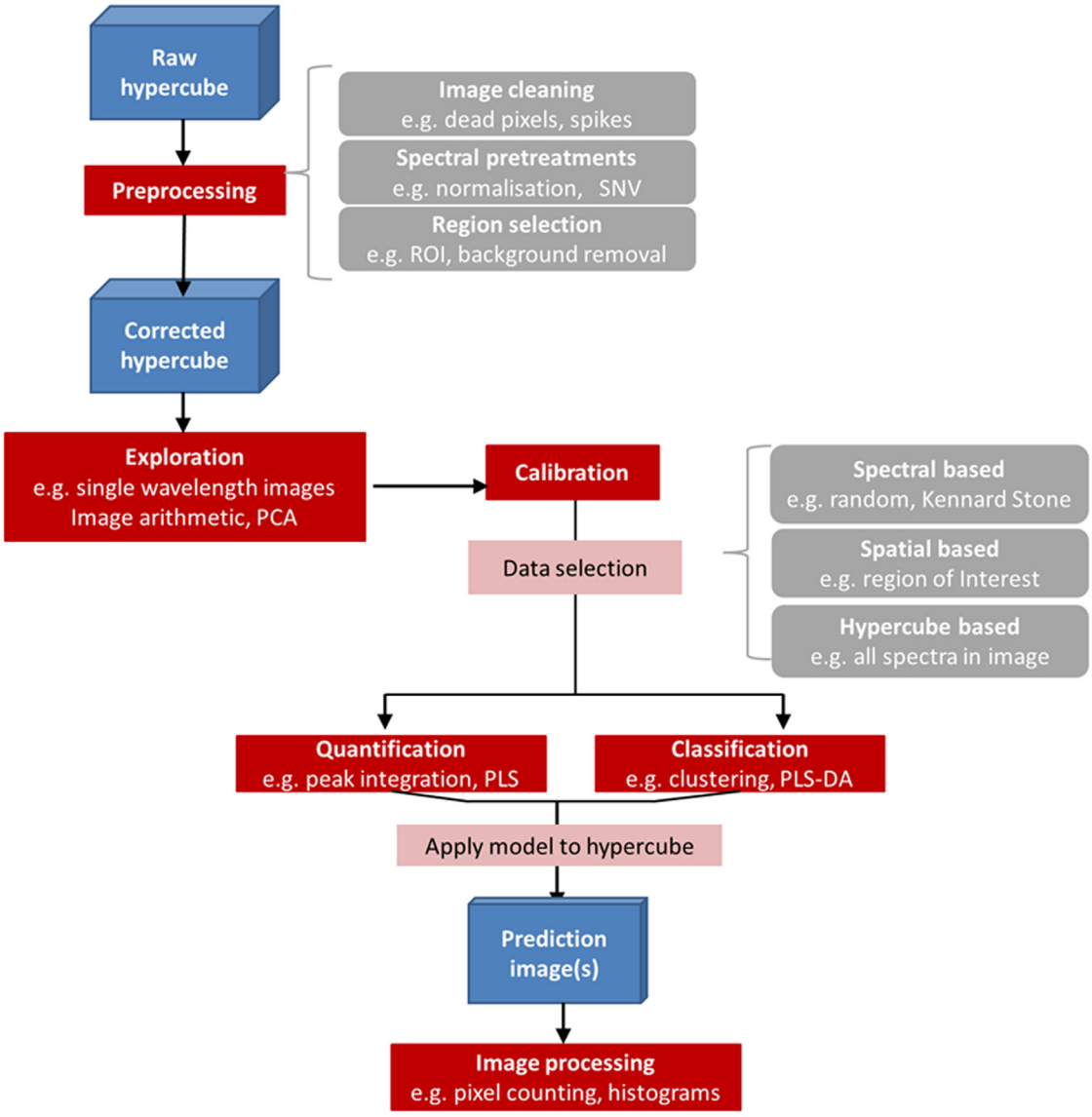

Fig. 2. Flow chart showing typical steps required in HSI data analysis.

Once the hypercube data has been preprocessed, the next data analysis step commonly carried out is exploratory analysis [25]. This may be as simple as examining single wavelength images at a wavelength corresponding to analytes of interest to estimate its spatial distribution on the sample. Image arithmetic, i.e. the combination of 2 or more waveband images (e.g. by addition, multiplication) to produce a new one is also possible. In the case of Raman imaging, where sharp peaks corresponding to specific chemical constituents are typically seen in the spectra, single wavelength images or integrated band images are often selected for visual analysis.

However, spectral bands in NIR and to some extent MIR tend to be broader and highly correlated, and it is often advantageous to use information from all wavelengths simultaneously. Multivariate data analysis or "chemometrics" is commonly applied for this purpose. Principal component analysis (PCA) is a basic chemometric approach useful for exploratory analysis of HSI data. An unsupervised technique, PCA enables the variance contained in the >100 image planes of a HSI data-cube to be reduced into a smaller number of PC score images. Each principal component is ordered in terms of decreasing contribution to the variance of the data, therefore PCA is a useful exploratory tool for summarising the main sources of variability in a hypercube.

While exploratory data analysis is a largely qualitative exercise, quantitative analysis is usually required, for example to classify pixels in order to test for the presence of a certain contaminant, or to estimate its concentration on a sample's surface. In order to quantify or classify hypercube data, it is necessary to develop a robust and reliable calibration model.

Within a hypercube, a given object could be represented by as many as 1000's of spectra. The analyst has the choice of selecting all or a portion of the spectra from each object. A subset of spectra could be extracted by selecting a spatial region of interest (ROI) from the image. An example of this process is shown in Fig. 3. Here, a trivial example of classifying apples and oranges is given to illustrate the concept. A square region of interest from each class is selected, and "dummy" variables of 0 and 1 are used to label the two classes. Alternatively it is possible to select a subset of spectra spanning the spectral domain, (e.g. using the Kennard and Stone algorithm [26]) however care must be taken to remove outlier spectra prior to applying this method.

Many algorithms are available for classification and quantification of pixels and/or objects in hyperspectral images. Unsupervised (e.g. k-nearest neighbours (kNN) and hierarchical clustering analysis (HCA)) and supervised methods (e.g. partial least squares

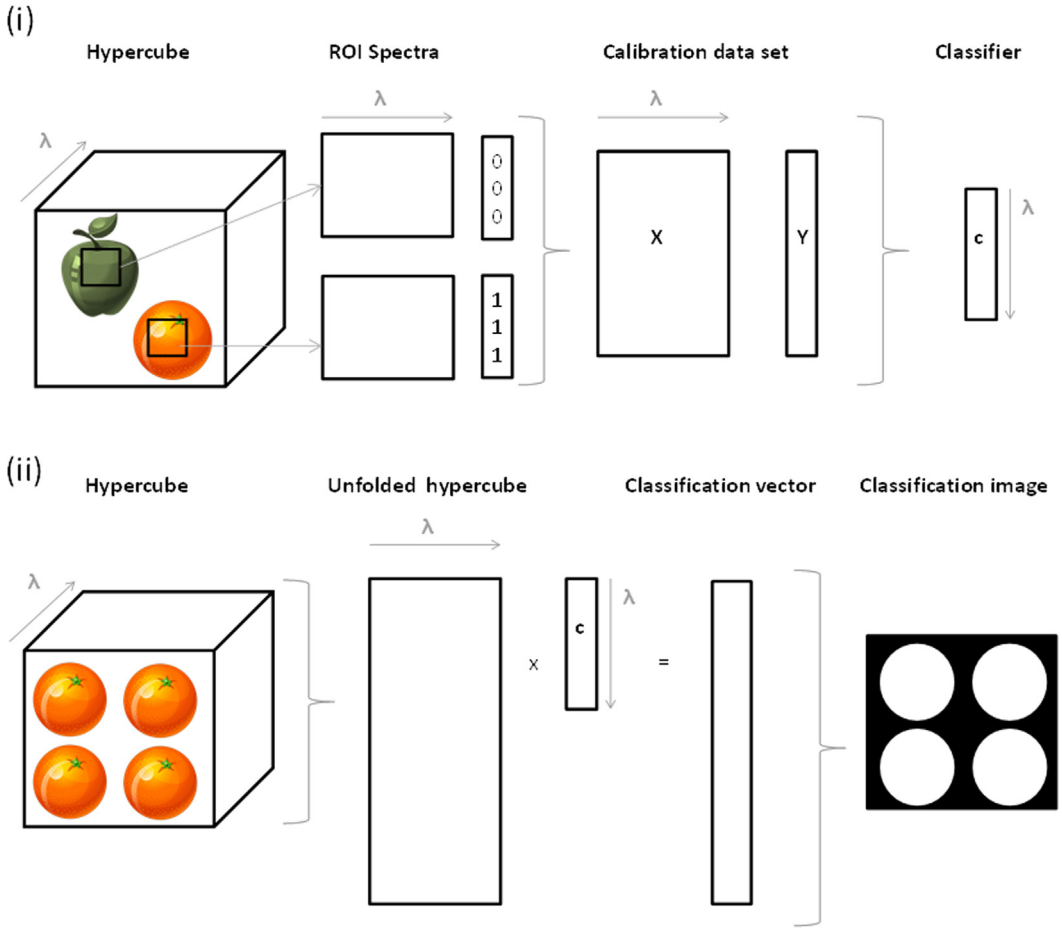

Fig. 3. Schematic showing: (i) development of classification model from hypercube data and (ii): application of classification model to new hypercube.

discriminant analysis (PLS-DA), linear discriminant analysis (LDA)) are often used for classification. Any classification model developed on spectral data can then be applied to each pixel spectrum in a hypercube, resulting in a prediction map, as shown in Fig. 3(ii).

A similar approach can be followed for quantitative modelling. However, quantitative models are rather more challenging than classification models when applied to HSI data, since reference values for analytes of interest are usually obtained on a per-sample basis. Indeed, obtaining reference values on a per-pixel basis is almost impossible. For this reason, when developing regression models for HSI data (e.g. using partial least squares regression (PLSR)), reference values are usually matched to a mean or median spectrum corresponding to an area of a sample on which the reference measurement was taken. Another quantitative modelling approach that overcomes some of the issues with reference values for quantitative modelling (as mentioned above) is multivariate curve resolution (MCR), which decomposes mixed spectra into several "pure" components. The proportion of pure components in a sample can then be quantified by pixel counting. This method is particularly powerful when pure component spectra are available, such as in hyperspectral chemical imaging of pharmaceutical excipients and active ingredients [27]. This approach could be useful for bacterial identification, if different microorganisms have sufficiently different spectral signatures.

Prediction models are typically evaluated by use of metrics such as the root mean squared error of calibration (RMSEC), cross validation (RMSECV) or prediction (RMSEP) and the coefficient of determination (R^2) [26].

4. Recent applications of chemical imaging for microbial characterization

In the following we discuss applications of hyperspectral chemical imaging for microbial characterization in the past 10 years. We subdivide reported applications as follows: Section 4.1: fundamental studies where HSI is used to gain information on biochemical processes of relevance to microorganisms; Section 4.2: applied studies where HSI is used to detect and identify microorganisms of concern at a microscopic scale, usually grown on "artificial" substrates such as stainless steel, silver or selective agars; Section 4.3: applied studies where HSI is used to detect microorganisms of concern at a macroscopic scale, grown on "real" substrates such as food or typical food preparation surface (e.g. formica).

For a more condense overview of current trends, these applications are further summarized by HSI modality in Table 1.

4.1. Fundamental studies

Microbial systems present specific challenges in HSI in terms of sample presentation. For example, water, a major component of microbial systems, exhibits high absorbance in the mid-infrared. Fourier transform infrared (FTIR) microscopy is one of the oldest lab-based HSI methodologies, but its application to microbial systems is quite limited. This is due to the strong light absorbance of water in the mid infrared wavelength range, which limits the signal obtainable [28]. To overcome this, Holman and co-workers

Table 1
Recent applications of HSI for microbial detection and classification.

Hyperspectral chemical imaging modality	Sample matrix	Wavelength range (nm)	Classification techniques applied	Type of microbe investigated	Reference
Vis–vNIR reflectance	Spinach	400–1000	Principal components analysis (PCA), artificial neural networks	*Escherichia coli*	[33]
Vis–vNIR reflectance	Mushrooms	400–1000	Partial least squares-discriminant analysis (PLS-DA)	*Pseudomonas tolaasii*	[34]
Vis–vNIR reflectance	Mandarins	320–1100	LDA, classification and regression trees (CART)	*Penicillum digitatum*	[32]
Vis–vNIR reflectance	Pork	400–1100	Multiple linear regression	*E. coli*	[42]
Vis–vNIR reflectance	Beef	400–1100	Multiple linear regression	Total viable counts (TVC)	[43]
Vis–vNIR reflectance	Beef	405–970	HCA, PLSR	TVC, *Pseudomonas* spp., and *Brochothrix thermosphacta*	[41]
Vis–vNIR reflectance	Chicken	400–1000	Wavelength band ratio	Fecal material and ingesta	[31]
Vis-vNIR Reflectance	Maize kernels	400–1000	PCA, DA	*Aspergillus*	[24]
Vis–vNIR reflectance	Chicken	400–1000	Interval PLS-DA, PLSR	TVC	[35]
Vis–vNIR reflectance	Rainbow agar	400–1000	Mahalanobis distance classifier	*E. coli*	[22]
Vis–vNIR reflectance	Rainbow agar	400–1000	PCA-DA, Mahalanobis distance classifier, kNN	*E. coli*	[23]
Vis–vNIR reflectance	Blood agar or Campy-Cefex agar	400–1000	PCA, Mahalanobis distance classifier	*Campylobacter*	[20]
Vis–vNIR reflectance	Blood agar or Campy-Cefex agar	400–1000	Thresolding, maximum likelihood classifier	*Campylobacter*	[21]
Vis–vNIR darkfield	Microscope slides	450–800	Direct spectral comparison	Biofilms of *E. coli and Salmonella enteritidis*	[16]
Vis–NIR reflectance	Salmon	400–1700	PLSR Least squares support vector machines (LS-SVM)	TVC	[48]
NIR reflectance	Aluminium well plates	1000-2350	Single band thresholding, PLS-DA	Series of Gram+, Gram−	[31]
NIR Reflectance	pork meat	900-1700	LDA, PLSR	TVC	[47]
NIR reflectance	Culture agar	1000–2498	PCA, PLS-DA	*Fusarium*	[37,38]
NIR reflectance	Chicken	900–1700	PLSR	*Enterobacteriaceae*	[46]
NIR reflectance	Chicken	900–1700	Stepwise PLSR	*Pseudomonas*	[49]
NIR reflectance	Chicken	900–1700	GA, PLSR	TVC	[50]
Fluorescence	Stainless steel	416–700	Wavelength band ratio	Biofilms of *E. coli, Pseudomonas pertucinogena, Erwinia chrysanthemi, Listeria Innocua*	[4]
Fluorescence	Stainless steel, HDPE, Formica	421–700	PCA, single & two-band selection	Biofilms of *E. coli*, *S. enteric*	[5]
FTIR transflectance	Biofilms on microfluidic cells	1800–1000 cm-1	Single wavenumber analysis	Biofilms of *E. coli*	[8]
Raman scattering	Water	3100–3703	Linear correlation with peak area	*Staphylococcus epidermidis, E. coli*	[10]
Raman scattering	Complex background matrix	2857–14285	PCA, hierarchical cluster analysis (HCA)	*Bacillus anthracis, Yersinia pestis, Burkholderia mallei, Francisella tularensis, Brucella abortus, ricin*	[29]
Raman scattering	Aliquot of bacteria with silver nanoparticles	5714–20000	PCA	*Bacillus thuringiensis vegetative cells, Bacillus anthracis spores*	[12]
Raman scattering	Distilled or recipe tap water	2857–20000	PCA, HCA	*Bacillus atrophaeus, B. thuringiensis, E. coli, Yersinia rhodei, Yersinia enterocolitica*	[11]
Raman scattering	Single bacterium	6250–50000	Peak integration	*Shewanella oneidensis*	[13]
Raman scattering	Biofilms on gold slides	6250–50000	Peak integration	*Biofilm of S. oneidensis*	[14]

[8] developed an FTIR-microscopic imaging system using a synchrotron light source and designed an open channel microfluidic system was constructed, which allowed a continuous laminar flow of thickness $< 15\ \mu m$ to maintain a viable bacterial community on the biofilm during image acquisition. The thinness of this layer, combined with the brightness of the synchrotron light source resulted in a SNR high enough to overcome the influence of water. With this system, it was possible to monitor the dynamics of biofilm formation and the response of *Escherichia coli* (*E. coli*) in biofilms to mitomycin (MMC) antibiotics. Marker peaks (1080, 1130, 1240, 1310 cm^{-1}) were selected for monitoring biofilm dynamics and time series analysis revealed that DNA-MMC adducts exhibit an infrared absorption band at $\sim$986 cm^{-1} related to vibration from the deoxyribose-phosphate backbone of the DNA-MMC adduct. Observation of chemical images at 1130 cm^{-1} enabled direct evidence that glycocalyx synthesis is prerequisite to the formation of bacterial biofilms. These studies are of importance on understanding some of the physiological changes taking place during the biofilm formation. Further research will be required focusing on other biofilm formers.

In contrast to FT-IR imaging, Raman imaging is less sensitive to the presence of water in aqueous samples. However, in many cases the Raman signal is weak, resulting in a low SNR. Significant signal enhancement can be achieved via surface enhancement, For example, in a recent study, gold nano-islands were used to enhance Raman scattering inside bacterial cells [13]. The nano-islands were introduced bacterial cells by culturing them in $HAuCl_4$ solutions. Raman HSI was then used to identify spatial locations of locate sites of intracellular chromate reduction within *Shewanella oneidensis (S. oneidensis)* cells with sub-micron spatial resolution. In a subsequent paper by the same group [14] the authors used a similar technique to monitor chromate, sulfate and nitrate localization sites and their interactions in *S. oneidensis* biofilms. The benefit of Raman scattering in these applications is the ability to select specific Raman shift wavenumbers corresponding to various chemical components in the sample, thus

facilitating detection and quantitation. In addition, Raman imaging can inherently achieve a greater spatial resolution than IR imaging, but often at the expense of longer acquisition times. As these techniques are complementary from both a spectral and spatial perspective, it is expected that combining the two methodologies would provide a more comprehensive understanding of the development and fate of bacterial biofilms.

4.2. Applied studies: Microscopic scale

The majority of microscopic HSI studies applied to microbiology have been carried out using Raman scattering, due to the inherently higher spatial resolution possible using this techniques ($\sim$1 μm) and its relative tolerance to water. As a consequence, Raman microscopic HSI has been applied for microbial assessment in a variety of matrices. In order to overcome the lengthy acquisition times associated with Raman microscopy, a number of solutions have been proposed. For instance, Escoriza and co-workers [10] used a Raman microscope to obtain an average Raman spectrum over the region of microbial cells (as identified in a brightfield image) for enumeration of waterborne pathogens *Staphylococcus epidermidis* (*S. epidermidis*) and *E. coli*. The Raman excitation wavelength employed was 532 nm and Raman scattering in the spectral range of 2800–3000 cm^{-1} (which contains the C–H stretching band) was used for quantification. In this paper, a number of different sampling approaches were investigated. Initially, *S. epidermidis* cell suspensions were transferred to an aluminum-coated slide and dried before Raman image acquisition. It was possible to count the bacterial cells directly from the brightfield image and these correlated well with integrated absorbance under the C–H stretching band ($R^2 > 0.99$ This showed the potential of the technique at high cell concentrations, but due to the typically low concentrations of bacterial cells in water, a prefiltration step was necessary. Thus, the subsequent sampling protocols investigated involved a pre-concentration step via membrane filtration. Inorganic filters (made from alumina or silver) were chosen rather than organic ones, to avoid background fluorescence in the Raman spectra. However, despite selecting inorganic filters, interference from the filter background still affected the observed Raman signals. For example, the alumina membrane produced significant background fluorescent signal that masked the Raman signal from the cells. Therefore it was necessary to photobleach the samples by irradiating the field of view for 15 min with the laser at 200 mW. After doing this a linear correlation (R^2=0.82) between the number of cells and the integrated area of the C–H peak was found. The silver filter performed relatively better than did the Alumina one. The C–H signal increased with cell concentration at concentration values exceeding 1×10^6 cells per membrane, and good correlation between integrated Raman intensity and reference measurements (e.g. standard plate counts, turbidity, dry weight) were found in the 2×10^6–2×10^8 cell/membrane range. Considering the limitations of the technique in terms of cell concentration, the authors note that a large quantity of water would need to be filtered in order to achieve a reliable Raman signal, thus limiting the practical application of the developed technique. It is therefore apparent that complex matrixes (like food) may limit the application of this technique while its potential might be more evident for microbial pathogens or spoilers that are critical at high concentrations.

In a later paper in 2008 [11], researchers used similar Raman imaging instrumentation to investigate the effects of various experimental and background interference parameters (i.e. laser-induced photodamage, water matrix and organism aging in water) on waterborne bacterial species identification. Gram-positive (e.g. *Bacillus atrophaeus (B. atrophaeus)*, *Bacillus thuringiensis*), Gram-negative (e.g. *Yersinia enterocolitica*, *Yersinia rhodei*, and *Pseudomonas fluorescens*) and protein suspensions were prepared in distilled or recipe water at a concentration of 1 mg/mL. The sample presentation was similar to one of those studied by Escoriza and co-workers [10]: 5 μL suspension was spotted onto aluminum-coated microscope slides and allowed to dry before Raman imaging. As expected, spores could withstand higher laser power density than their vegetative counterparts before photodamage occurred. All studied organisms could accommodate laser power densities less than 2300 W/cm^2 without substantial photodamage. The Raman spectra were classified according to species and genus using Hierarchical cluster analysis of Mahalnobis distance between principal component scores of spectral data in the C–H (2800–3100 cm^{-1}) and fingerprint (600–1800 cm^{-1}) regions. Excellent species-level classification was reported, due to the uniqueness of each Raman spectrum, regardless of age or water matrix tested (sensitivity > 95%, specificity > 99%). Mixtures of *B. atrophaeus* and *E. coli* suspensions (prepared in a 1:9 weight ratio) were also investigated to show the imaging as well as the spectral capability of Raman imaging and the possibility of classifying individual spores and cells was demonstrated. Similarly to the previous techniques, further applications will be required in non-aqueous samples for assessing its potential in other microbiological studies.

Another approach to improving the efficiency of Raman HSI is to use a multi-modal approach, as presented by Kalasinksy and co-workers [29] at the United States Armed Forces Institute of Pathology (Pennsylvania, USA). This research team developed a novel chemical imaging system integrating Raman spectroscopy, fluorescence spectroscopy and digital imaging for detecting low levels of pathogens in complex background matrixes, including common white powders, pharmaceutical drugs, excipients, explosives, industrial solvents, toxic industrial chemicals. Samples were imaged on aluminium coated microscope slides (powder samples were deposited on the slides, materials in suspension or solution were dropped on the slide and allowed to dry at room temperature and drug samples were dissolved in methanol before deposition). A hierarchical approach was developed to extract useful information from each modality in the detection system. Optical imaging was used for identifying the boundaries of target particles, fluorescence imaging for rapid screening of large surface areas to detect biological particulates (since biological materials exhibit auto-fluorescence under UV excitation). After combined analysis of morphology and fluorescence, suspect pathogen particles were then analyzed with Raman imaging. The rationale of this hierarchical approach is clear: to use rapid techniques (i.e. optical imaging and fluorescence) to obtain detailed spatial information from larger sample areas and identify potential contaminants, followed by the more lengthy yet specific Raman acquisition. PCA was employed as a data reduction step prior to cluster analysis, correlation analysis, and data visualization. The identity of an agent was evaluated by calculating the Mahalanobis distance between a test spectrum and classes defined within the Raman signature library. Further studies will be required to assess its potential for developing other pathogen signature libraries.

Surface enhanced Raman scattering (SERS) has been applied to enhance the SNR of Raman chemical images of bacterial cells: Guicheteau and co-workers [12] compared SERS with conventional Raman imaging for analysis of bacterial mixtures. Aqueous suspensions of mixtures containing various *Bacillus* (*B.*) species cells and spores (e.g. *B. thuringiensis*, *Bacillus anthracis* and *Bacillus cereus*) were dropped on Aluminum slides and allowed to dry at room temperature. Samples for SERS measurement were mixed with an aliquot of silver colloids before measurement. Raman chemical images were obtained using a laser excitation wavelength of 532 nm and principal component analysis was applied to each hypercube to discriminate between different species, cells and spores. Use of SERS improved both signal to noise ratio (by a factor of 10) and the time required to obtain each hypercube (by a factor of 60), due to the signal enhancements achieved. The

procedure of preparing the samples appears to be the major time consuming challenge of this technique.

Other sub-micron scale applications have relied on dark-field illumination. This method allows only light scattered from the sample to reach the detector, thus enhancing the contrast between small objects, such as cells, and backgrounds, such as suspension fluids. Advantages of this technique as compared to FTIR and Raman imaging are: fast acquisition times (e.g. 1 min per hypercube), low energy light source (i.e. minimal interference with sample through heating or photodegradation) and insensitivity to water. Park and co-workers [30] applied this technique in the visible wavelength range to characterize the spectral and spatial profiles of *Salmonella enteritidis* (*S. enteritidis*) and *E. coli*. Live cells, mounted on microscope slides and covered with coverslips, were investigated data spatial resolution of approximately 0.45 μm within a field of view of $100 \times 100\ \mu m^2$.The movement of live cells during imaging resulted in some blurring; nevertheless, systematic spectral differences were observed for the two bacteria where *E. coli* exhibited lower scattering intensity and fewer peaks than did *S. enteritidis*. *S. enteritidis* biofilms exhibited several spectral peaks at 458, 494, 522, 550, 574, 590, and 670 nm while the only dominant spectral peak found for *E. coli* biofilm was found at 546 nm. Differences like these in the spectral character could be used to create a library for future biofilm classification. An important issue pointed out in this paper is that some parameters of the hyperspectral microscopic imaging system (e.g., integration time, gain and light source) had a strong influence on bacterial hyperspectral images and that it is essential to optimize these in order to reduce minimize noise. For example, an integration time lower than 250 ms was recommended to avoid signal saturation from biofilms formed by *S. enteritidis*. Another challenge of darkfield illumination in HSI of cells is the necessity to use a high intensity light source, which could damage cells. In general, optimization of HSI system parameters such as light or laser intensity and integration time is of crucial importance and preliminary experiments should be carried out to ensure acceptable SNR is achieved without substantially interfering with the sample.

4.3. Applied studies: Macroscopic scale

4.3.1. Bacteria grown on agar, deposited on aluminum or stainless steel plates

One of the first research studies on the application of macroscopic scale NIR HSI for microbial detection and identification published in 2005, In this study, it was shown that NIR reflectance images (in the wavelength range 1200–2350 nm) could be used for differentiating bacteria deposited in aluminium well-plate. Each well was 2 mm deep and 1 mm in diameter and after deposition, suspensions were allowed to dry for 15 min. Gram positive bacteria (*Listeria monocytogenes*, *Listeria innocua*, *B. subtilis* and *B. cereus*) were successfully identified and separated from Gram negative bacteria (*E. coli* and *Salmonella* spp.) based on the intensity of their second derivative spectra [31]. Both single waveband and partial least squares discriminant analysis were investigated for classification. The combination O–H stretch at 1940 nm due to water was useful for discrimination between gram positive and negative species, probably due to the difference in protection from dehydration provided by the outer membrane. The band at 1685 nm, related to *cis*-double bonds in unsaturated fatty acids, allowed isolation of *B. cereus*. However, it was not possible to distinguish between all 5 bacteria investigated using just one waveband, so the authors proposed a multistep procedure by sequentially thresholding the image at 2190, 1400 and 1900 nm. PLS-DA, employing the full wavelength range, resulted in excellent classification all of the species. Further studies on biological surfaces will be of interest in order to identify the optimal wavebands for similar or other type of bacteria.

Hyperspectral fluorescence imaging has been evaluated for the detection of microbial biofilms grown on stainless steel plates (to mimic the typical surfaces of food processing equipment) using a portable hyperspectral fluorescence system developed by researchers at the USDA [4]. Biofilm features were enhanced by forming a band ratio image of 444/588 nm. In a follow-up paper [5], the authors report the use of a lab-based hyperspectral fluorescence system to detect microbial bio-films (*E. coli* and *Salmonella enterica)* on a variety of food contact surfaces such as stainless steel, high density polyethylene (HDPE), plastic laminate (Formica), and polished granite. Biofilm formation was encouraged on these surfaces by deposition of culture suspensions followed by incubation in sterile chambers at 22 °C for 3 days. Following incubation, samples were dried at room temperature for 1 hour. Hyperspectral fluorescence images were then acquired from 421 to 700 nm using ultraviolet-A excitation. In order to overcome auto-fluorescence typical of most biological materials, the biofilms were grown in M9 medium, which exhibits minimal autofluorescence. It was possible to distinguish biofilm formation on stainless steel, HDPE and granite using band ratio images. However, a high false positive rate was reported for the Formica samples, which may be related to the lower cell population density of biofilms grown on this type of surface (4.3–6.4 log cfu cm^{-2}). Although in general the results of this study are promising for the detection of biofilms grown in M9 medium, it is unclear whether the auto-fluorescence typical of most biological materials would reduce the effectiveness of this method in real samples.

Yoon and co-workers [32] investigated the application of visible and near infrared reflectance HSI for detection of *Campylobacter* colonies directly on agar plates. Eleven *Campylobacter* strains and six non-*Campylobacter* bacterial strains were cultured in broth at 42 °C for 72 h and then inoculated onto mainly two types of culture agars, namely, blood agar and Cefex agar. To avoid confluent growth of colonies, well-separated point inoculation was implemented with 5 μL aliquots at each assigned site. These inoculated plates were then incubated for up to 48 h before the grown colonies were imaged. Savitzky–Golay smoothing was applied to each individual spectrum to reduce noise and then PCA loadings together with the Bhattacharyya distance measure were used determine an optimal waveband image for classification of *Campylobacter* colonies, non-*Campylobacter* colonies and agars. Based on the image at 503 nm for Blood agar samples a simple threshold method was found to discriminate the three classes. However, for classification of *Campylobacter*-colonies, non-*Campylobacter* colonies and Cefex agar in Cefex-agar-based samples at 501 nm, a second step involving a Mahalanobis distance classifier was required. In both cases, classification accuracy of over 99% was attained. The same research group reported early detection of *Campylobacter* colonies in a subsequent paper [33]. Bacterial strains were handled the same way as described above but with a shorter incubation time of 24 h. In order to assess the potential of this technique, further in vitro and in situ studies will be required in the future.

Due to the lack of appropriate selective agar, the identification of non-O157 serogroups is always problematic. Recently, researchers investigated the use of Vis–vNIR HSI for the detection and classification of six non-O157 Shiga-toxin producing *E. coli* (STEC) serogroups (026, 045, 0103, 0111, 0121 and 0145) grown as “spots” on Rainbow agar [34]. Spectral libraries were created by selecting regions of interest in the hyperspectral images representing the different classes and classification was carried out using the supervised Mahalanobis distance classifier. When applied to an independent test set, the developed models worked well for classification of serogroups 045 and 0121, however, the results were less promising for classification of the other serogroups. This was due to the confounding influence of spectral variability

induced by variations in growth media and variations in STEC populations in the test set images. In order to overcome these issues, in later work, this research team investigated the use of the spread plate technique [23]. Classification was much improved using this technique, with reported correct classification percentage for cross validation ranging from 84 to 100%. Nevertheless, the method will need to be validated in more biotic or abiotic surfaces for assessing its potential in other realistic environments.

Various species of fungi (e.g. *Aspergillus flavus, Aspergillus parasiticus, Aspergillus nigerniger* and *Fusarium* spp.) are of concern in the food industry due to the potential for production of toxic secondary metabolites, i.e. mycotoxins. Del Fiore and co-workers [36] investigated the potential of Vis–vNIR HSI (in the 400–1000 nm wavelength range) for identifying maize kernels inoculated with various fungal species. In addition to imaging maize kernels, the authors examined fungal mycelia grown on potato dextrose agar. The authors reported that the spectral characteristics of *Aspergillus* strains were different from each other, especially in the visible region of the spectrum. This is to be expected, since colour is a major factor in discriminating these species when they are examined by traditional methods. However, it was found that colour variation also existed among different maize hybrids, which may confound discrimination of fungi on the surface of kernels. To overcome this, the authors suggest that the spectral range beyond 600 nm should be used for classification of fungal contamination. That the spectral variation observed was due to variations in maize water content was ruled out by examining kernels with different moisture profiles. Using the full wavelength range (400–1000 nm), non-inoculated and inoculated maize kernels could be discriminated between after 2 days, using a principal components/linear discriminant analysis chemometric approach.

Williams and co-workers [37,38] recently applied macro-scale NIR HSI for investigation of members of the *Fusarium* (*F.*) genus and analysis of their growth characteristics. By using PCA, these researchers were able to examine variation in the NIR spectral response of pixels from different species and variations among strains within each species. NIR HSI diffuse reflectance images of *Fusarium* colonies grown on potato dextrose agar were obtained and PLS-DA was applied to the data for classification of the three species. Although the PLS-DA model could discriminate between *F. subglutinans* and *F. proliferatum*, it was not capable of discriminating between *F. verticillioides* and the other species, due to the large spectral variation observed within that class. Further optimization studies will be required in order to assess the potential of NIR HCl for fungi discrimination between the same or different species.

4.3.2. Bacteria on food surfaces

Identification, classification and quantitation of microbial growth directly on food surfaces would allow early detection of potential microbial contamination. As previously discussed, great progress has been made in the past 10 years in microscopic HSI of bacteria at the single cell and biofilm level. However, using techniques such as FTIR and Raman microspectrometry to monitor growth directly on the food surface is unfeasible due to instrumental challenges, including lengthy data acquisition times, small sample area, fluorescence from the food matrix and signal saturation due to high water content. Macroscopic HSI in the Vis–NIR wavelength range overcomes many of these challenges. Typically two wavelength ranges, i.e., 400–1000 nm (visible to very near infrared, or Vis–vNIR for brevity) and 900–1700 nm (NIR) have been investigated (this is due to the relatively widespread availability of CCD detectors for the Vis–VNIR range) and InGaAs detectors for the NIR). However, the overtone and combination molecular vibrations encountered in the NIR are overlapped and thus assignment of NIR wavelengths is challenging. Nevertheless, Vis–NIR HSI has shown much potential for detecting secondary effects of microbial growth or detection of suspect contamination on food samples. For example, fecal materials are directly linked with the presence of coliforms, and so, due to the relatively high prevalence of food borne illness associated with consumption of contaminated chicken, there has been a substantial research effort in the use of HSI to detect fecal and ingesta contamination on chicken carcasses [39–42].

An early paper on this topic [43] introduced Vis-vNIR (460–1020 nm) HSI for detection of damage caused by the growth of *Penicillium digitatum* on mandarins. The mandarins were inoculated with a suspension of *P. digitatum* spores for 3 days. Pixel spectra were selected from the hyperspectral images and labelled as belonging to one of four classes (healthy skin, rotten skin, sporulated skin and stem) based on human inspection. Chemometric methods such as linear discriminant analysis and genetic algorithms were tested for classification of the pixel spectra. Although classification of pixels is a common step in HSI data analysis, in food quality monitoring it is more commonly required to classify entire objects. In this study, the authors classified samples as damaged if they had more than 5% damaged pixels. It was possible to classify correctly more than 90% of the inoculated samples using just 20 wavebands. The potential of using fewer wavebands for detection is interesting as these could potentially be used to develop a low cost multispectral imaging system.

In later studies, Vis–vNIR HSI was employed to detect microbial contamination on horticultural products such as spinach leaves inoculated with *E. coli* [44] and mushrooms inoculated with *Pseudomonas tolaasii* [3]. The hypothesis of such studies is that the metabolic activity of the inoculated microorganism would result in biochemical changes with the concurrent formation of metabolic by-products, which could potentially be detected by HSI, thus indicating contamination. It is also important to be able to distinguish between such changes and the normal biochemical changes that occur over the shelf life of food (e.g. enzymatic browning). In the mushroom study [34] bacterial and enzymatic activity both resulted in the development of brown pigments on the mushroom surface, however, using the spectral information it was possible to differentiate between physically and microbial-induced damage with $>95\%$ classification rates.

The total viable count (TVC) of microbes on various of poultry, meat and fish products have also been estimated using by using HSI. For example, Grau and co-workers [35] investigated the use of visible HSI to study the freshness of chicken fillets during storage at 4 °C. Using 13 wavebands, an RMSEP of 0.73 log CFU g^{-1} was reported. Feng and Sun [46] carried out a similar study in the NIR wavelength range, establishing both full wavelength and simplified models (based on selected wavelengths) in the NIR range. In that study, the distribution of bacterial loads on meat surfaces was visualized by producing pseudo-color images where different colors indicate different levels of bacterial loads as shown in Fig. 4. However, it is important to note that the development of prediction maps relies on the quality of raw images and more importantly on the robustness of the calibration models. This can be evaluated using independent test sets for model verification.

Barbin and co-workers [47] used NIR HSI to classify pork samples (*longissimus dorsi* muscles) stored at 0 °C and 4 °C into two categories (fresh and spoiled in terms of their bacterial loads) using linear discriminant analysis (LDA) and quantified TVC loads using PLSR. Wu and Sun [48] studied visible and near-infrared (400–1700 nm) hyperspectral reflectance imaging for prediction of TVC on salmon fillets. The developed prediction models exhibited excellent performance, with an $R^2 > 0.98$. Since many quality changes in foods, including TVC, colour and moisture content are correlated with storage time, it is essential to randomize the order of image acquisition with respect to storage day. In addition, it is of importance to assess the potential of this technique on specific bacteria apart from the TVC.

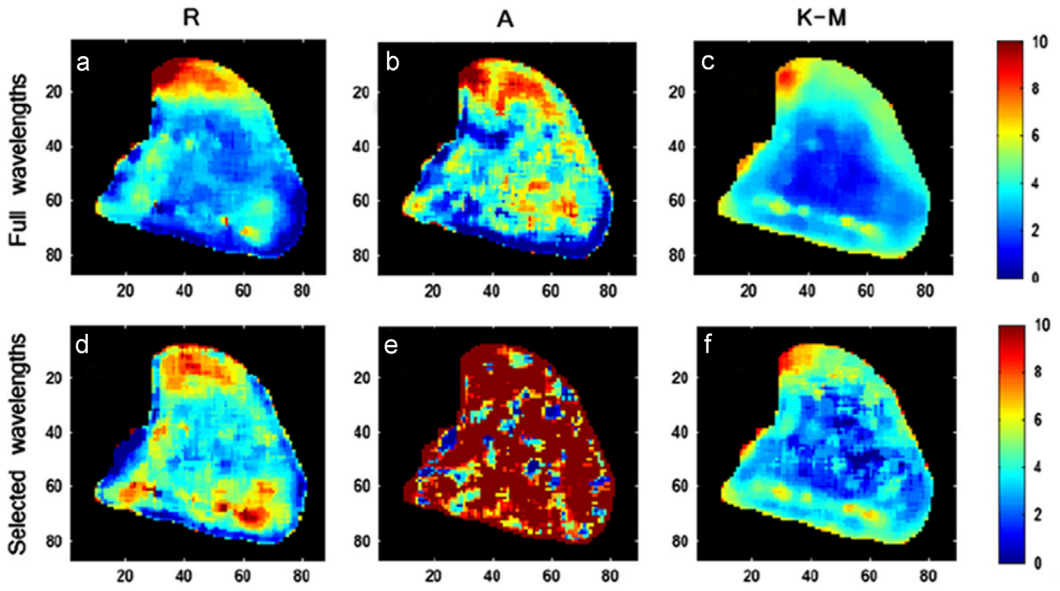

Fig. 4. Prediction maps for TVC in one chicken sample by applying PLSR models based on different spectral parameters (taken from reference [46]).

Besides predicting the total number of bacteria, it is also of great interest to detect specific bacterial genera/groups so that more insights can be given to better understand the ecology of bacteria and thus facilitate development of effective technologies for food safety control. To determine *Enterobacteriaceae* loads in chicken fillets, Feng and co-workers [49] compared two wavelength selection methods (second derivative and regression coefficients based) in order to establish a PLSR prediction model. The prediction maps showed clear increasing trends of *Enterobacteriaceae* loads over storage at 4 °C. *Pseudomonas spp*. and *Brochothrix thermosphacta* (*B. thermosphacta*) are the dominant bacteria during meat spoilage process if meat is stored under aerobic conditions. Feng and Sun [50] later employed a pushbroom HSI system (900–1700 nm) to determine the loads of *Pseudomonas spp.* on chicken breast fillets. The authors proposed a wavelength selection scheme based on genetic algorithms, which was useful to allocate important wavelengths for model calibration and prediction. Panagou et al. [51] worked on beef meat stored at both chill and abuse temperature (0, 4, 8, 12, and 16 °C) and utilized a multispectral imaging system (18 wavelengths in 405–970 nm) with LED light source to analyze meat freshness as well as to predict the microbial counts of beef samples. The images were taken in an area-scanning manner where a single-band image was acquired while the LED light source at that specific wavelength was activated. The study showed that this system could classify samples with TVC loads of >7 log CFU $g^{-1}$from those with fewer bacteria. The prediction of *Pseudomonas spp* and *B. thermosphacta* was also good with $R>0.9$.

Spatially-resolved hyperspectral scattering is another variant of HSI, which involves illuminating a sample at a specific location and obtaining line scans at different distances from the light beam. This method provides information on the light scattering properties of the sample and has been applied in the 400–1100 nm wavelength range to predict *E. coli* contamination on pork [52]. Pork samples were dipped into bacterial suspensions of different *E. coli* concentration (10^2 up to 10^{10} cfu/mL). Multiple linear regression was applied to the scattering profiles and a correlation coefficient of cross validation of 0.84 was reported. A similar technique was developed to measure biochemical changes occurring within fresh beef due to the formation of metabolites caused by bacterial growth [53]. Experiments were performed on samples with total viable counts ranging from 5 to 9 $\log_{10}$ cfu/g and a standard error of prediction of 0.3 $\log_{10}$ cfu/g was reported.

5. Summary of main challenges associated with HSI of microbial samples

This review demonstrates the potential of HSI as a tool for microbiology, to gain fundamental understanding of microbial processes and rapid detection/identification on a variety of substrates. However, high set-up costs and difficulties with high-speed data acquisition and processing still limits the widespread industrial application of HSI [42]. After reviewing the main applications of HSI to microbiology a number of key challenges, common to many if not all of the HSI modalities covered, can be summarized as follows.

5.1. Sample presentation

In microscopic FTIR and Raman studies, different sample presentation techniques have been proposed to overcome issues such as signal interference by water or low microbial concentration. The simplest solution to water interference is to dry samples prior to imaging [10,11]. However, the drying process greatly alters the sample and is thus not advisable for studies on dynamical processes such as biofilm formation. Some researchers have overcome this issue through the use of novel microfluidic cells to ensure a thin layer of aqueous samples combined with a high intensity synchrotron light source [8]. The use of ATR-FTIR imaging is another means of overcoming the dominating influence of water absorption in aqueous samples, however the full potential of ATR imaging has not yet been realized in this area, although studies on animal cells using ATR have shown much promise [6]. However, as the authors of [8] point out, the penetration depth of light in an ATR-FTIR is approximately 1 μm, and thus mainly surface information can be obtained. This approach may however be interesting for the study of microbial attachment to modified surfaces.

Darkfield HSI is another emerging technique that enables imaging of live bacterial cells in the native environment. However, when imaging live cells there is a large risk of image blurring due to cell motility.

Considering macroscopic samples, where the objective of HSI is online monitoring of microbial contamination, sample presentation is required to be simple and straightforward. A more pressing concern in such applications is the ability to obtain information

from the whole sample. This issue has been addressed by the use of mirrors for imaging greater surface areas of apples [54].

5.2. Spatial resolution

Spatial resolution is a key limiting parameter in HSI applied to microbiology, for fundamental studies, the spatial resolution of the system defines the smallest cell or region that can be examined. Typical FTIR imaging systems have a spatial resolution of around 20 μm, although this can be reduced using special optical arrangements, such as ATR. This limits the use of FTIR HSI for the study of individual bacterial cells, which as usually smaller than 1 μm. However, the growth dynamics of larger bacterial colonies are accessible using this technique. Raman imaging can achieve a pixel size down to 500 nm or less, which makes it possible to examine cells. In addition, superresolution techniques can be applied to improve the spatial resolution even further [55].

Similarly, in detection of contamination on macroscopic samples, the spatial resolution of the system used defines the smallest area of microbial growth that can be detected on a sample. Typical macroscopic Vis–NIR systems have a spatial resolution of approximately 300 μm. This means that in some cases, contaminated samples with small colonies may be un-detected. However, a compromise between pixel resolution, the field of view imaged and the speed of image acquisition must always be found.

5.3. Limit of detection

Another challenge for HSI is the quantification of microbes at low concentrations. Current studies have focused on assessing the spoilage of food products or identifying microbial levels which are higher than 10^2 cfu/mL. These studies will need to be expanded to more bacterial species. Some limitations may appear in relation to the lowest bacterial level of detection that might be higher of what traditional plating techniques may achieve. Applications may be limited to bacteria that have an impact on the food safety and quality at high microbial loads. The development of highly specific discriminating approaches to pick out particular organisms is also another challenge to be considered in future developments. This becomes more difficult when dealing with co-cultures that are present in fermented food products. In these cases a macroscopic in tandem with a microscopic/nanoscopic assessment may need to be applied. Previous knowledge of the bio-products of the studied microorganisms will help to establish correlations with these by-products and the presence and level of bacterial contamination. Future developments in HSI technology should improve the efficiency of the microscopic and the direct macroscopic assessments.

5.4. Speed of image acquisition

The relatively long sample acquisition times needed to produce a hyperspectral image (up to a few hours) in the case of Raman HSI is one of the major drawbacks of this technique. In the case of biofluorescence emission, process time may be increased as an additional period is required to photobleach biological samples prior to data collection in order to reduce the sometimes overwhelming biofluorescence emission [12]. The physical shutter mechanisms and the quantum efficiencies of the charge-coupled device cameras makes difficult the adjustment of the exposure time for effective high-speed imaging of moving targets. An exposure time setting ideal for a shorter wavelength image often causes image saturation at a higher wavelength. Nevertheless, current electron-multiplying charge-coupled device (EMCCD)-based cameras, which have high quantum efficiencies and use rapid frame-transfer mechanisms can significantly improve the signal to noise ratio [40].

Acknowledgements

The first author acknowledges funding from the EU FP7 under the ERC starting grant.

References

[1] D. Wu, Da-Wen Sun, Innov. Food Sci. Emerg. Technol. 19 (2013) 1–14.
[2] ⟨http://www.newport.com/Quartz-Tungsten-Halogen-Lamps/378263/1033/info⟩.aspx. Accessed on 18/12/2014.
[3] E. Gaston, J.M. Frias, P.J. Cullen, C.P. O'Donnell, A.A. Gowen, J. Near Infrared Spectroscop 18 (2010) 341–353.
[4] W. Jun, K. Lee, P. Millner, M. Sharma, K. Chao, M.S. Kim, 2008. in: Food Processing Automation Conference, ASABE, USA. 1, 1-6.
[5] W. Jun, M.S. Kim, B. Cho, P.D. Millner, K. Chao, D.E. Chan, J. Food Eng. 99 (2010) 314–322.
[6] M.K. Kuimova, K.L. Chan, S.G. Kazarian, Appl. Spectrosc. 63 (2009) 164–171.
[7] L. Miller, M. Smith, Vibr. Spectrosc. 38 (2005) 237–240.
[8] HY1. Holman, R. Miles, Z. Hao, E. Wozei, LM. Anderson, H. Yang, Anal. Chem 81 (2009) 8564–8570.
[9] S. Yang, B. Li, M. Slipchenko, A. Akkus, N. Singer, Y. Yeni, O. Akkus, J. Raman Spectrosc. 44 (2013) 1089–1095.
[10] M. Escoriza, J. VanBriesen, S. Stewart, J. Maier, P. Treado, J. Microbiol. Method 66 (2006) 63–72.
[11] A. Tripathi, R.E. Jabbour, P.J. Treado, J.H. Neiss, M.P. Nelson, J.L. Jensen, A.P. Snyder, Appl. Spectrosc. 62 (2008) 1–9.
[12] J. Guicheteau, S. Christesen, D. Emge, A. Tripathi, J. Raman Spectrosc. 41 (2010) 1632–1637.
[13] S.P. Ravindranath, K.L. Henne, D.K. Thompson, J. Irudayaraj, ACS Nano 5 (2011) 4729–4736.
[14] S.P. Ravindranath, Ulhas S. Kadam, D.K. Thompson, J. Irudayaraj, Anal. Chim. Acta 745 (2012) 1–9.
[15] P. Magnan, Nuclear Instrum. Methods Phys. Res. A 504 (2003) 199–212.
[16] J. Phang, D. Chan, S. Tan, W. Len, K. Yim,L. Koh, C. Chua, L. Balk, 2005. A review of near infrared photon emission microscopy and spectroscopy, in: IEEE Proceedings of 12th IPFA 2005, Singapore, 275–281.
[17] Characteristics and Use of Infrared Detectors, Hamamatsu. ⟨http://www.hamamatsu.com/resources/pdf/ssd/infrared_techinfo_e.pdf⟩.
[18] A.A. Gowen, F. Marini, C. Esquerre, et al., Anal. Chim. Acta 705 (2011) 272–282.
[19] T. Isaksson Naes, T. Fearn, T. Davies, A User Friendly Guide to Multivariate Calibration and Classification, NIR Publications, 2002.
[20] J. Burger, A. Gowen, Chemometr. Intell. Lab. Sys. 108 (2011) 13–22.
[21] J. Burger, P. Geladi, J. Chemometr. 19 (2006) 355.
[22] J. Burger, NIR News 20 (7) (2009) 19.
[23] C. Esquerre, A. Gowen, C.P. O'Donnell, G. Downey, Chemometr. Intell. Lab. Sys 117 (2012) 129–137.
[24] T. Fearn, C. Riccioli, A. Garrido-Varo, J.E. Guerrero-Ginel, Chemometr. Intell. Lab. Sys 96 (2009) 22–26.
[25] J. Amigo, I. Marti, A. Gowen, Chemometr. Food Chem., Elsevier (2013) 343.
[26] D. Massart, Handbook of Chemometrics and Qualimetrics Part 2 (1998) 372.
[27] F. Franch-Lage, J.M. Amigo, E. Skibsted, S. Maspoch, J. Coello, Int. J. Pharm. 411 (2011) 27–35.
[28] M. Baker, J. Trevisan, P. Bassan, R. Bhargava, H. Butler, K. Dorling, P. Fielden, S. Fogarty, N. Fullwood, K. Heys, C. Hughes, P. Lasch, P. Martin-Hirsch, B. Obinaju, G. Sockalingum, J. Sulé-Suso, R. Strong, M. Walsh, B. Wood, P. Gardner, F. Martin, Nat. Prot. 9 (2014) 1771–1791.
[29] K.S. Kalasinksy, T. Hadfield, A.A. Shea, V.F. Kalasinsky, M.P. Nelson, J. Neiss, A. J. Drauch, G.S. Vanni, P.J. Treado, Anal. Chem. 79 (2007) 2658–2673.
[30] B. Park, S.C. Yoon, S. Lee, J. Sundaram, W.R. Windham, A. Hinton Jr, K.C. Lawrence, Trans. ASABE. 55 (2012) 1997–2006.
[31] J. Dubois, E. Lewis, F. Fry, E. Calvey, Food Microbiol. 22 (2005) 577–583.
[32] Yoon, et al., Trans. ASABE 52 (2009) 651–662.
[33] Yoon, et al., Food Qual 4 (2010) 35–49.
[34] W.R. Windham, S.C. Yoon, S.R. Ladley, G.W. Heitschmidt, K.C. Lawrence, B. Park, N. Narang, C.C. William, J. Near Infr. Spectrosc. 20 (2012) 547–558.
[35] S.C. Yoon, W.R. Windham, S.R. Ladely, J. Near Infr. Spectrosc. 21 (2013) 81–95.
[36] A. Del Fiore, M. Reverberi, A. Ricelli, F. Pinzari, S. Serranti, A. Fabbri, Int. J. Food Microbiol. 144 (2010) 64–71.
[37] Paul J. Williams, Paul Geladi, Trevor J. Britz, et al., Appl. Microbiol. Biotechnol. 96 (2012) 803–813.
[38] Paul J. Williams, Paul Geladi, Trevor J. Britz, et al., Anal. Bioanal. Chem. 404 (2012) 1759–1769.
[39] B. Park, K. Lawrence, W. Windham, D. Smith, J. Food Eng. 75 (2006) 340–348.
[40] K. Chao, C. Yang, M.S. Kim, D.E. Chan, Appl. Eng. Agric. 24 (2008) 475–485.
[41] K. Chao, C. Yang, M.S. Kim, J. Food Proc. Eng 34 (2011) 125–143.
[42] S.C. Yoon, B. Park, K.C. Lawrence, W.R. Windham, G.W. Heitschmidt, Comp. Electron. Agric 79 (2011) 159–168.
[43] Gomez-Sanchis, L. Gomez-Chova, N. Aleixos, G,C. Camps-Valls, J. Montesinos-Herrero, E. Molto, J. Blasco, J. Food Eng. 85 (2008) 191–200.
[44] U. Siripatrawan, Y. Makino, Y. Kawagoe, S. Oshita, Talanta 85 (2011) 276–281.
[46] Y.-Z. Feng, D.-W. Sun, Talanta 105 (2013) 244–249.
[47] D. Barbin, G. ElMasry, D.-W. Sun, P. Allen, N. Morsy, Innov. Food Sci. Emerg. Technol. 17 (2013) 180–191.

[48] D. Wu, D.-W. Sun, Talanta 111 (2013) 39–46.
[49] Y.-Z. Feng, G. ElMasry, D.-W. Sun, A. Scannell, D. Walsh, N. Morcy, Food Chem. 138 (2013) 1829–1836.
[50] Y.-Z. Feng, D.-W. Sun, Talanta 109 (2013) 74–83.
[51] E.Z. Panagou, O. Papadopoulou, J.M. Carstensen, G.-J.E. Nychas, Int. J. Food Microbiol. 174 (2014) 1–11.
[52] F. Tao, Y. Peng, Y. Li, K. Chao, S. Dhakal, Meat Sci. 90 (2012) 851–857.
[53] Y. Peng, J. Zhang, W. Wang, Y. Li, J. Wu, H. Huang, X. Gao, W. Jiang, J. Food Eng. 102 (2011) 163–169.
[54] D. Reese, A. Lefcourt, M. Kim, Y. Lo, Bioresour. Technol. 100 (19) (2009) 4499–4506 (06/2009).
[55] L Duponchel, P Milanfar, C Ruckebusch, J. Huvenne, Anal. Chim. Acta. 607 (2007) 168–175.